PHYSICAL REVIEW C VOLUME 22, NUMBER 4 OCTOBER 1980

Cross sections for the ^{6}Li(^{3}He,p) reaction at energies below 2 MeV

A. J. Elwyn, R. E. Holland, C. N. Davids, J. E. Monahan, F. P. Mooring, and W. Ray, Jr.
Argonne National Laboratory, Argonne, Illinois 60439
(Received 9 June 1980)

Absolute cross sections for the ^{6}Li(^{3}He,p) reaction to the ground, 2.94-, 16.63-, and 16.92-MeV states in ^{8}Be, as well as for the total underlying proton continuum, have been obtained for incident ^{3}He energies between ~0.5 and 1.85 MeV. Differential and total (integrated) reaction cross sections with accuracies of 10–20 % are presented. Thermonuclear reaction-rate parameters are calculated. Interpretation of the observed proton and alpha particle continuous spectra is discussed.

[NUCLEAR REACTIONS ^{6}Li(^{3}He,p)^{8}Be, ^{6}Li(^{3}He,p)2α, $E_{^3\mathrm{He}}$ = ~0.5–1.85 MeV; enriched LiF target; measured $\sigma(E_{^3\mathrm{He}},\theta)$, $\sigma(E_{^3\mathrm{He}})$; calculated $\langle\sigma v\rangle$.]

I. INTRODUCTION

In this paper, we report the determination of both total and differential cross sections for various outgoing proton channels that result from reactions of ^{3}He with ^{6}Li at bombarding energies below 2 MeV. This work is part of an ongoing series of measurements[1-3] of absolute reaction cross sections for light ions with ^{6}Li. It has relevance to the structure of light nuclear systems such as ^{8}Be and ^{5}Li. At the same time, it provides, along with the results of previous studies,[3] part of the data base necessary for the evaluation of the p-^{6}Li advanced fuel cycle which has been suggested[4-6] as a minimum neutron-producing alternative for the possible future generation of fusion power reactors.

Contributions to the proton spectra from ^{3}He + ^{6}Li reactions arise from a number of processes. Monoenergetic, or nearly monoenergetic, groups are associated with reasonably narrow energy levels in ^{8}Be. At the same time, a continuum of proton energies results from the breakup of broader ^{8}Be states into two α particles, the decay of ^{5}Li states [formed in the ^{6}Li(^{3}He,α) reaction] into a proton and α particle, and the direct three-body breakup process, $^3\mathrm{He} + {}^6\mathrm{Li} \rightarrow 2\alpha + p$. While such spectra have been studied[7] a number of times, absolute cross sections have with only a few exceptions been given for the ground and first excited ^{8}Be states alone. Schiffer *et al.*[8] have measured absolute excitation functions as well as a number of angular distributions for these two groups at energies between 0.9 and 5.1 MeV. Angular distributions as well as integrated cross sections were obtained by Gould and Boyce[9] from 3–6 MeV, along with the first absolute estimate of the cross section for direct three-body breakup. Fletcher *et al.*[10] report cross sections for the ground and first-excited ^{8}Be states at energies between 5 and 17 MeV normalized to the data of Ref. 8. Differential cross sections for the production of the 16.63 and 16.92 MeV ^{8}Be levels at energies between 3.5 and 4.25 MeV are given by Erskine and Browne.[11]

The present experiments were undertaken to provide more complete and accurate data at energies between 0.5 and 2.0 MeV. In particular, we report absolute cross sections for the ^{6}Li(^{3}He,p) reaction to the ground (Q = 16.788 MeV), 2.94-, 16.63-, and 16.92-MeV states in ^{8}Be, as well as values associated with the continuous proton energy distribution (Q = 16.880 MeV). We also obtain fragmentary data on the deuterons from the ^{6}Li(^{3}He,d) reaction to the ground and first-excited state in ^{7}Be.

The experimental technique is briefly reviewed in Sec. II, and the results, including tabulated reaction cross sections, are given in Sec. III. Interpretation of the observed proton and α-particle spectra, and thermonuclear reaction-rate parameters are presented in the final section.

II. EXPERIMENT

The experiments were performed at the Argonne 4-MV Dynamitron accelerator. The techniques have been discussed in previous reports;[1-3] specific procedures for the present measurements are reviewed below.

The accelerated ^{3}He beam entered a 76-cm diam scattering chamber through two defining apertures. The targets, placed at the center of the chamber, were thin films (25–40 μg/cm^2) of LiF enriched to 99.3% in ^{6}Li, evaporated on various backing materials. Charged particles produced in the reaction were detected by collimated 2000 μm thick Si surface-barrier detectors mounted on movable arms within the chamber. The beam line and target-chamber system were pumped by

liquid-nitrogen trapped turbomolecular pumps and a liquid-nitrogen cooled sorption trap to typical chamber pressures of less than 10^{-6} Torr. The beam entered the target chamber through an in-line liquid-nitrogen cold finger before impinging upon the targets. In general, carbon contaminant buildup on the ^{6}LiF targets was low, but even so, targets were replaced frequently, particularly for those runs in which absolute cross sections were determined. The Dynamitron energy scale was calibrated[12] at the neutron threshold (1.8806 MeV) in the $^{7}Li(p,n)^{7}Be$ reaction, and at the 872.11 and 340.46 keV resonances in the $^{19}F(p,\alpha\gamma)^{16}O$ reaction.

Because of the nature of the processes contributing to proton spectra from $^{3}He + ^{6}Li$ reactions, we performed the measurements in two distinct parts. In the first step, the angular distribution of protons corresponding to the formation of ^{8}Be in its ground state was determined. The thin ^{6}LiF films were evaporated on thick (0.0025–0.0075 cm) Ta disks, so that beam currents up to 200 nA could be employed to increase statistical accuracy without rupturing the targets. Two detectors covered with thin Al foils to stop elastically scattered ^{3}He particles were used to collect the data, while a third fixed at a back angle served as a monitor. The pulses from the detectors were amplified and digitized with 1024 channel analog-to-digital converters interfaced to a PDP-11/45 computer; these were stored as pulse-height data and later transferred to magnetic tape. Angular distributions for the ground state protons were determined at laboratory angles between 0 and 155 degrees, at energies from 0.46 to 1.85 MeV. Absolute differential cross sections were determined by normalization to separately measured 45 and 135 degree excitation functions. For these latter measurements, the thin ^{6}LiF layers were evaporated on 10 $\mu g/cm^2$ C foils, and the beam passing through the targets was collected in a Faraday cup in which secondary electron loss was magnetically suppressed. Total charge was measured with a current integrator, accurate to $\lesssim 0.5\%$, and corrections[1] for the altered charge state of the beam passing through the thin foils as well as for effects due to small-angle multiple scattering were applied. The thickness of the targets was determined from measurements of the energy loss of back-scattered protons and alpha particles, as described earlier,[3] by use of atomic stopping powers tabulated by Anderson and Zeigler[13] and Zeigler.[13] Previous experience[1,3] has shown that target thicknesses measured by this technique always agreed within 5% with the thickness inferred from Rutherford scattering.

In the second part of these measurements, the ^{3}He beam from the accelerator was pulsed, and the masses of the outgoing reaction products were identified by time-of-flight techniques. The post-accelerated beam-pulse rate was 8 MHz, pulse width about 1 ns, and flight path from the thin carbon-backed targets to the detector about 20 cm. Time and pulse height data from the single movable Si detector (with Al foils removed) used in these measurements were stored as a two-dimensional array in the computer, and later transferred to magnetic tape. Angular distributions were determined at laboratory angles between 35 and 155 degrees for incident ^{3}He energies from 0.66 to 1.85 MeV. For each set of data, the time-vs-energy two-dimensional array was transformed to a mass-vs-energy matrix as described previously,[2] and individual pulse-height spectra for the various outgoing particle masses could be selected. Typical total and mass-selected spectra are shown in Fig. 1. Protons associated with the ground, 2.94-, 16.63-, and 16.92-MeV states in ^{8}Be are clearly identified. The nonzero yield below the peaks arise from various continuum contributions. The dashed vertical lines indicate the maximum energy for protons and alpha particles from the breakup of ^{8}Be and ^{5}Li states as indicated. It should be mentioned that in spectra such as those in Fig. 1, the energy of the protons extends from 17 or 18 MeV (depending on bombarding energy and detector angle) down to zero. The need to determine flight times over this large dynamic range, coupled with the very large yields associated with the elastically scattered ^{3}He particles, limited the low-energy mass resolution in the time-of-flight method. The lowest energy proton that could be accurately identified usually corresponded to a value just above the elastic ^{3}He peak. Thus, contributions to the proton spectrum at energies below this peak often could not be measured and an extrapolation procedure, based on the assumption that no lower energy relatively narrow proton groups exist,[14] had to be employed in order to determine proton continuum yields.

Proton yields for each of the observed excited ^{8}Be states were obtained relative to the ground state by determining the net areas under the peaks. In this procedure, the underlying continuum yields were subtracted using a linear approximation; this constituted a source of systematic uncertainty in the peak areas, particularly for broad peaks such as the one at 2.94 MeV, even when the subtraction was performed in a completely consistent manner. Such uncertainties were included in estimates of the absolute errors. Relative yields associated with the continuum contributions were determined by integrating the spectra from energies just above the 16.63-MeV state peak up to the maximum proton energy, subtracting the net con-

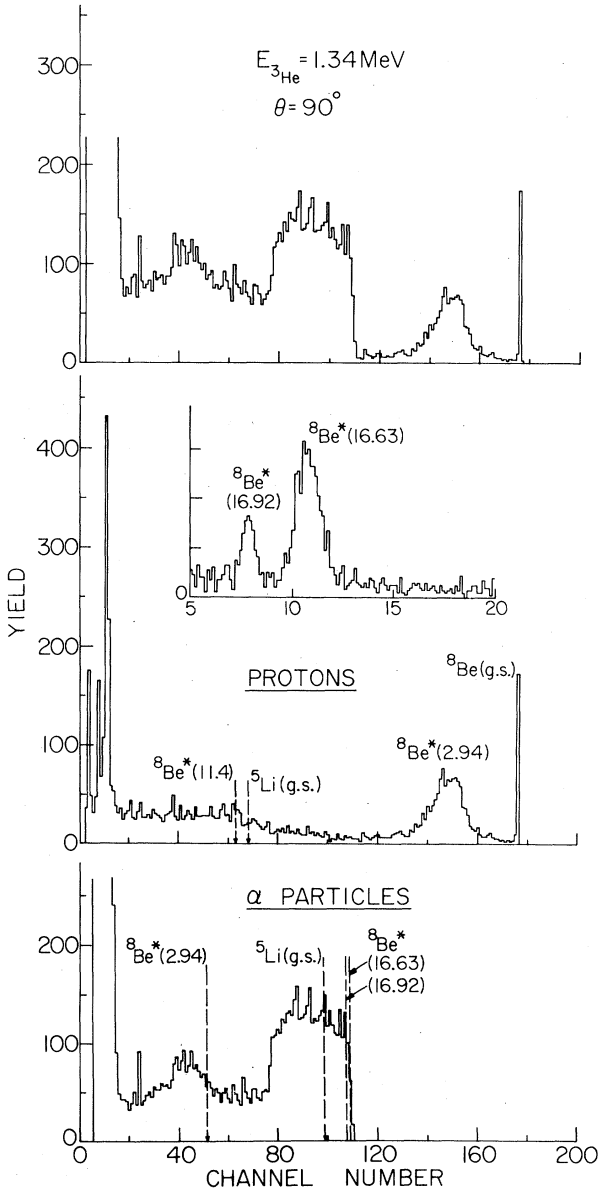

FIG. 1. Pulse-height spectrum of charged particles from $^6Li + ^3He$ reactions at an incident energy of 1.34 MeV and laboratory angle of 90°. The top part shows the total spectrum, the center section the spectrum of protons after mass selection (the inset represents an expansion of channels 5–20), and the mass-selected alpha particle spectrum is indicated on the bottom. The vertical dashed lines indicate the maximum energy for protons and alpha particles from the breakup of ^8Be and ^5Li energy levels.

tribution from the ground and 2.94-MeV states, and adding the counts based on a reasonable extrapolation to zero energy where the yield should be zero. This latter addition constituted, at most, 15% of the total continuum yield. The method was checked at those bombarding energies and laboratory angles at which it was possible to integrate the continuous yield from a somewhat lower proton energy—a value below the 16.92-MeV state—where the extrapolated portion was at most 1–2% of the total, and both results agreed very closely. In determining the errors associated with the total continuum yield, an uncertainty of 50% of the extrapolated counts was included.

Absolute cross sections for the various contributions to the total proton yield were found at each energy and angle by normalization to our previously measured ^8Be ground state values. It should be noted that the continuum cross sections, determined as indicated above, include protons that arise from the expected broad state in ^8Be at 11.4 MeV, the sequential breakup of ^5Li formed in the $^6Li(^3He, \alpha)$ reaction, and from any direct three-body breakup contribution. The term "continuum" is used in the following sections to describe this continuous contribution to the total proton reaction cross section.

III. RESULTS

Angular distributions in the center-of-mass system are presented in Figs. 2–5 for the ground, 2.94-, 16.63-, and 16.92-MeV ^8Be states, and in the laboratory system for the continuum protons in Fig. 6, at each average ^3He bombarding energy. These energies differ from the incident energy because of energy loss[15] in the ^6LiF targets. The error bars represent relative uncertainties based on the usual methods of propagating errors due to counting statistics.

The solid curves on Figs. 2–6 result from fitting the differential cross section to a series of Legendre polynomials at each energy. The coefficients B_L in the expansion are listed in Tables I and II. Integrated (reaction) cross sections (i.e., $\sigma_r = 4\pi B_0$) are also shown in Tables I and II, and plotted as a function of incident energy in Fig. 7. Both the relative errors (indicated by the ± values) and the absolute uncertainties (shown in parentheses as percentages) are indicated in the Tables I and II. Absolute uncertainties were obtained by combining statistical with systematic errors in quadrature. Included as systematic uncertainties are estimates of the errors in the number of events in spectrum peaks relative to those in the underlying continuum background and uncertainties in yields obtained by extrapolation, as well as errors in target thickness, total charge determination, and detector solid angles.

Figure 8 shows the cross sections to the ground and 2.94-MeV states in ^8Be obtained in the present experiment. They appear to be lower than the

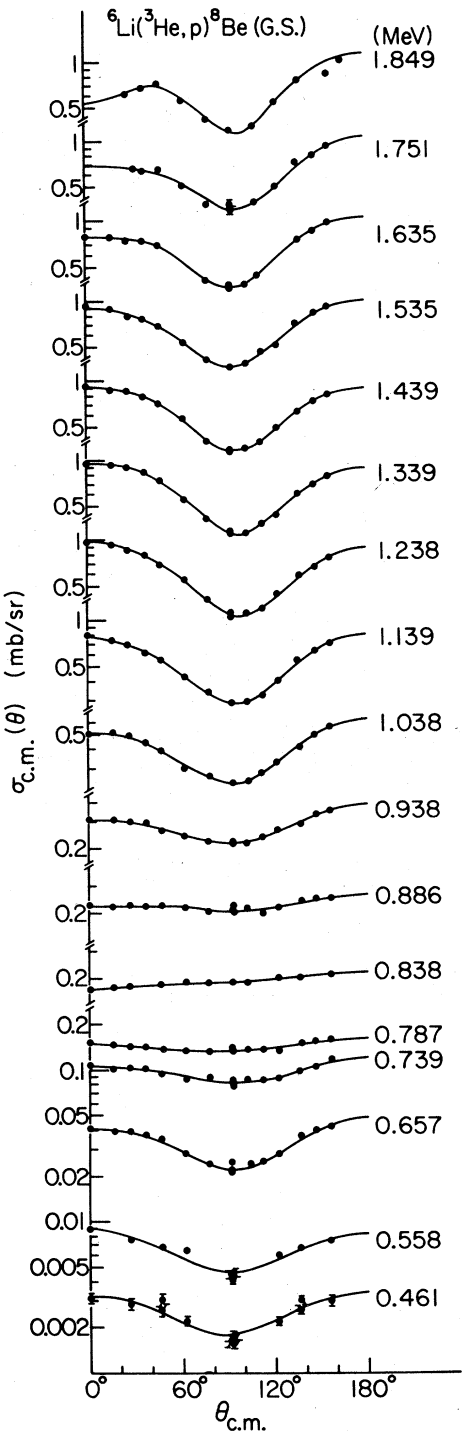

FIG. 2. Angular distribution in the center of mass of the protons from the ^{6}Li(^{3}He,p)^{8}Be, (g.s.) reaction at the average ^{3}He energies indicated. The smooth curves represent the results of the Legendre polynomial fits. Relative errors are indicated by the bars or the size of the points.

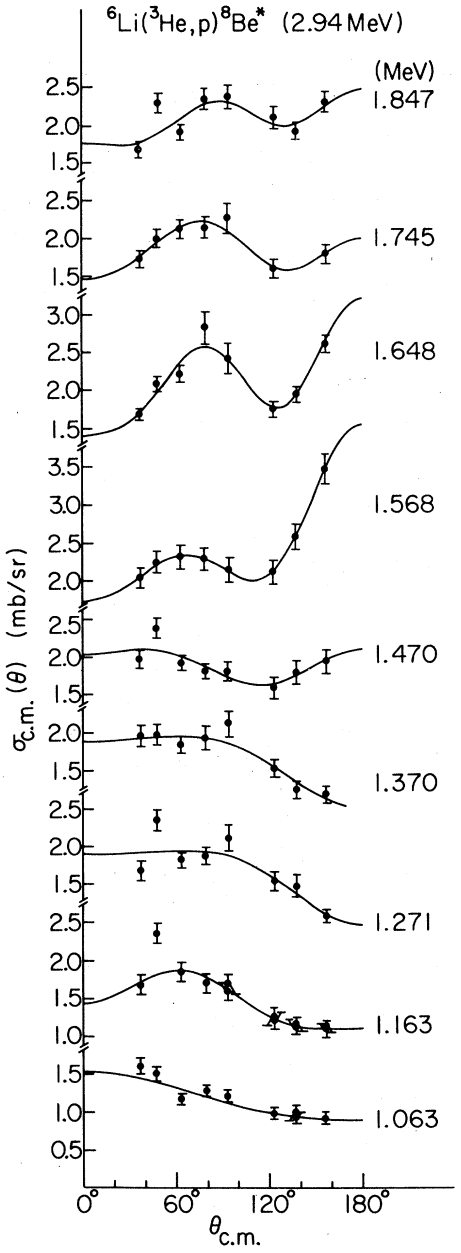

FIG. 3. Angular distribution in the center of mass of the protons from the ^{6}Li(^{3}He,p)^{8}Be*(2.94-MeV) reaction at the average ^{3}He energies indicated. The smooth curves represent the results of the Legendre polynomial fits. The error bars represent relative uncertainties. Angular distributions measured at energies between 0.66 and 0.949 MeV are not shown.

trend of the earlier measurements[8] although the region of overlap is small. The points[9] marked "three-body breakup" represent an estimate of the direct three-body breakup cross section obtained by assuming that the shape of the continuum is given by three-body phase space only. Our con-

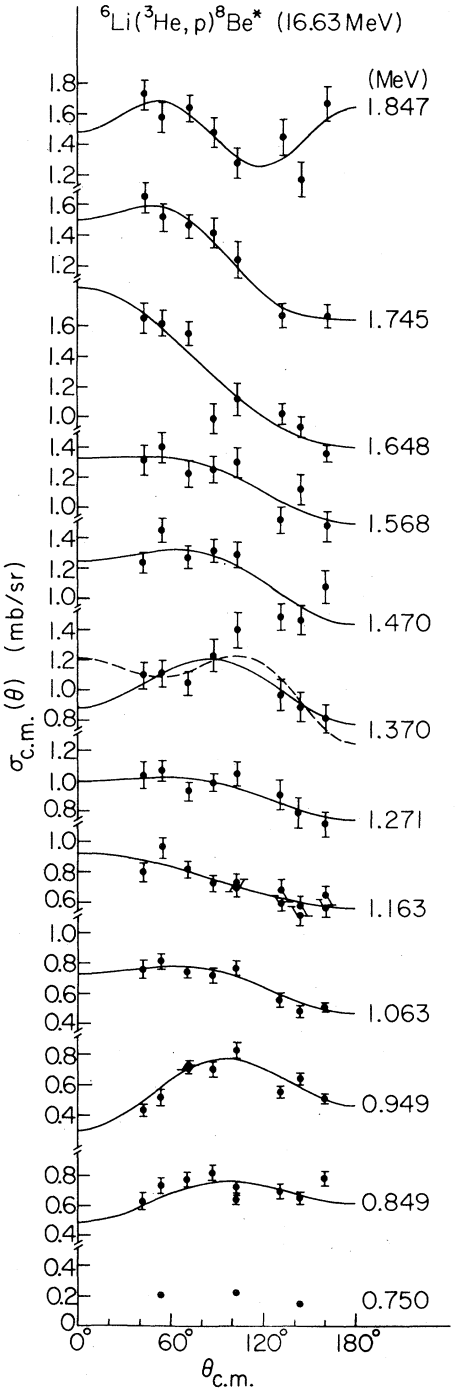

FIG. 4. Angular distribution in the center of mass of the protons from the ^{6}Li(^{3}He,p)^{8}Be* (16.63-MeV) reaction at the average ^{3}He energies indicated. The smooth curves represent the results of the Legendre polynomial fits. (At 1.37 MeV the solid curve is a 3-polynomial fit while the dashed curve shows the fit for 4 polynomials. The values for B_0 are equal within the accuracy of the fits.) The error bars represent relative uncertainties.

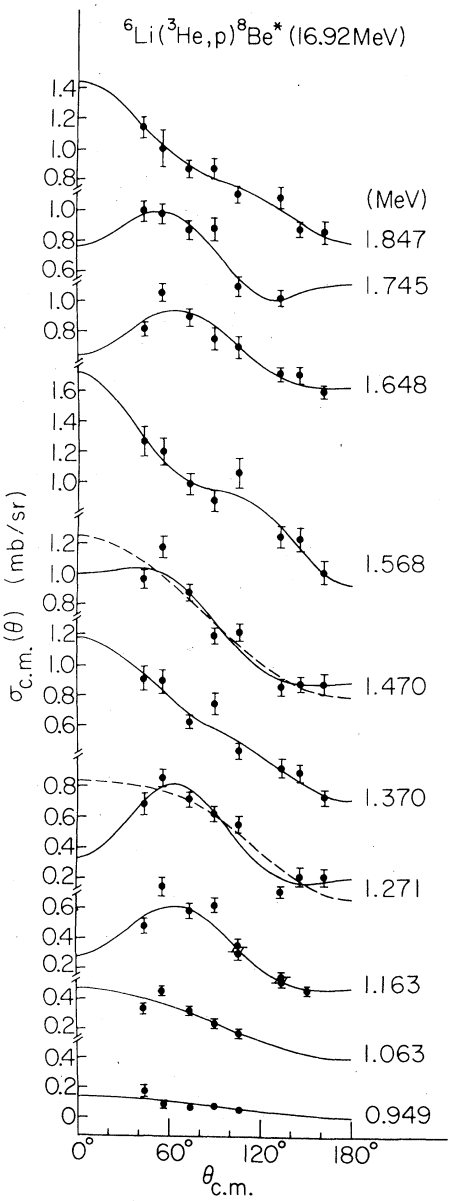

FIG. 5. Angular distribution in the center-of-mass of the protons from the ^{6}Li(^{3}He,p)^{8}Be* (16.92-MeV) reaction at the average ^{3}He energies indicated. The smooth curves represent the results of the Legendre polynomial fits. (At 1.271 and 1.470 MeV the solid curves are 4-polynomial fits while the dashed curves show the fits for 3 polynomials. The values for B_0 are equal within the accuracy of the fits.) The error bars represent relative uncertainties.

tinuum cross sections, as we have described them above, include contributions from the very broad 11.4-MeV ^{8}Be state and the breakup of ^{5}Li as well as direct breakup, and should therefore be larger.

Barr and Gilmore[16] have measured cross sections for the ^{6}Li(^{3}He,d)^{7}Be reaction by an activation

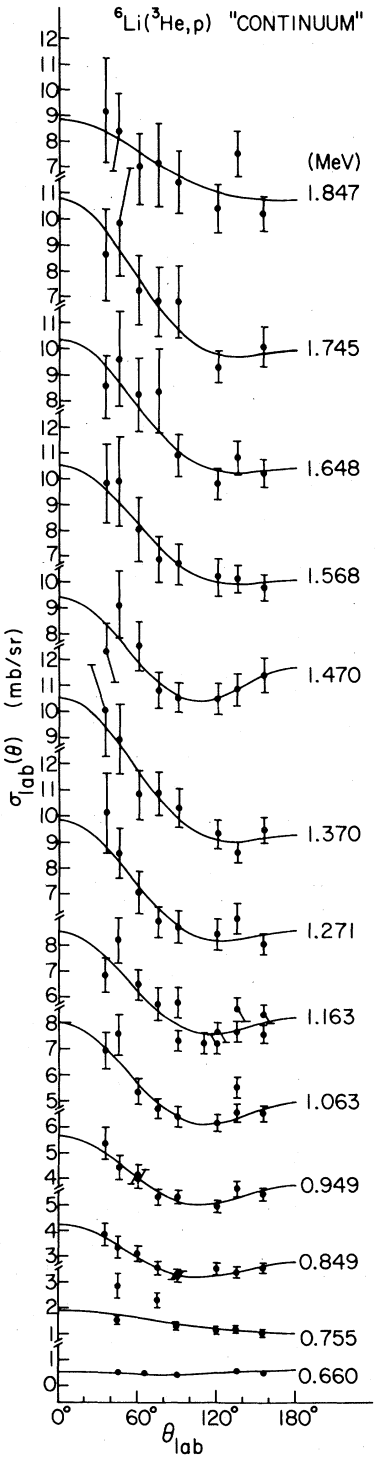

FIG. 6. Angular distribution in the laboratory system of the continuum protons in ^{3}He+^{6}Li reactions at the average ^{3}He energies indicated. The smooth curves represent the results of the Legendre polynomial fits. The error bars represent relative uncertainties.

technique. Although our experimental time-of-flight procedures were not optimized for selection of mass-2 particles (of low energy), it was possible to observe the spectra of outgoing deutrons (at least at forward angles) for some bombarding energies. Such spectra exhibited two peaks corresponding to the formation of ^{7}Be in its ground and first excited states, the only states in ^{7}Be stable against particle decay. From cross sections determined at laboratory angles $\lesssim 90°$, center-of-mass angular distributions indicated near isotropy for both groups. With the assumption of isotropy, total reaction cross sections for the sum of the two groups were obtained, and are indicated in Fig. 9. They are in excellent agreement with the activation measurements of Barr and Gilmore[16] whose experimental method was completely different.

IV. DISCUSSION

A. Proton and α-particle energy spectra

The mechanism that describes the formation of three-body channels in reactions of ^{3}He with ^{6}Li can be approximated by an incoherent superposition of sequential decays through states in ^{8}Be and ^{5}Li along with a contribution from direct three-body breakup. As seen in Fig. 1, the proton energy spectrum at energies greater than 1 MeV (channels $\gtrsim$12) appears to be dominated by α-α final-state interactions in the ground (0^+), 2.94-MeV (2^+), and perhaps the 11.4-MeV (4^+) states in ^{8}Be. Although it is not obvious in the figure, protons from the secondary breakup of ^{5}Li formed in the ^{6}Li(^{3}He,α) reaction and from direct three-body breakup may contribute as well. For α particles the interpretation is not as clear, although one expects that the p-α final state interaction to the $p_{3/2}$ and $p_{1/2}$ states in ^{5}Li must contribute along with α particles from the secondary breakup of the various ^{8}Be states (2.94, 16.63, and 16.92 MeV) formed in the first stage reaction, and again some contributions from direct three-body decays.

We have performed calculations in an attempt to interpret the observed spectral shapes more quantitatively. For two-step (sequential) reactions of the form

$$\begin{array}{l} A+B \rightarrow C+D \\ \qquad\quad \hookrightarrow F+G\,, \end{array} \tag{1}$$

the shape of the energy spectrum of outgoing particles D that can be attributed to final-state interactions between F and G can be written[17] as

$$N_l(E) = P_{C-D} \sum_{lj} C_{lj} \left[\frac{\sin^2(\delta_{lj}+\phi_l)}{P_l}\right]_{F-G}, \tag{2}$$

TABLE I. Values of coefficients B_L in the expansion of the differential cross section for the ^{8}Be ground state (in the c.m. system) into a series of Legendre polynomials $[\sigma(\theta) = \sum_L B_L P_L(\cos\theta)]$ and the reaction cross section σ_r, where $\sigma_r = 4\pi B_0$. The errors are relative uncertainties generated in the fitting program and do not include systematic errors.

$E_{^3\mathrm{He}}$ (MeV)	B_0 (mb/sr)	B_1 (mb/sr)	B_2 (mb/sr)	B_3 (mb/sr)	B_4 (mb/sr)	σ_r[a] (mb)
0.461	0.0023±0.0001	−0.0001±0.0001	0.0010±0.0001			0.029±0.001(20)
0.558	0.0059±0.0001	0.0002±0.0002	0.0026±0.0003			0.074±0.001(15)
0.657	0.030 ±0.003	−0.001 ±0.001	0.015 ±0.001	−0.003±0.001		0.38 ±0.04(15)
0.739	0.093 ±0.001	−0.003 ±0.002	0.020 ±0.002	−0.005±0.003		1.17 ±0.01(10)
0.787	0.140 ±0.001	−0.007 ±0.002	0.015 ±0.002	0.0 ±0.003		1.76 ±0.01(10)
0.838	0.193 ±0.001	−0.028 ±0.002	0.005 ±0.003	−0.005±0.003		2.425±0.013(9.5)
0.886	0.222 ±0.002	−0.012 ±0.004	0.025 ±0.004	−0.012±0.006		2.79 ±0.03(9.5)
0.938	0.264 ±0.001	−0.023 ±0.002	0.091 ±0.003	−0.019±0.004		3.32 ±0.01(9.5)
1.058	0.351 ±0.002	−0.019 ±0.004	0.224 ±0.005	−0.036±0.006		4.41 ±0.03(9.5)
1.139	0.458 ±0.003	0.026 ±0.005	0.337 ±0.005	−0.048±0.007		5.75 ±0.04(9.5)
1.238	0.535 ±0.004	0.102 ±0.007	0.396 ±0.007	−0.06 ±0.01		6.72 ±0.05(9.5)
1.339	0.556 ±0.002	0.106 ±0.004	0.399 ±0.005	−0.069±0.006	−0.028±0.007	6.98 ±0.03(9.5)
1.439	0.562 ±0.003	0.067 ±0.006	0.389 ±0.006	−0.061±0.008	−0.035±0.009	7.06 ±0.04(9.5)
1.535	0.582 ±0.005	−0.001 ±0.008	0.40 ±0.01	−0.06 ±0.01	−0.02 ±0.01	7.31 ±0.06(9.5)
1.635	0.573 ±0.004	−0.046 ±0.008	0.385 ±0.008	−0.09 ±0.01	−0.06 ±0.01	7.20 ±0.05(9.5)
1.751	0.560 ±0.007	−0.06 ±0.01	0.36 ±0.02	−0.13 ±0.02	−0.02 ±0.03	7.04 ±0.09(10)
1.849	0.575 ±0.008	−0.08 ±0.02	0.36 ±0.02	−0.22 ±0.03	−0.10 ±0.03	7.23 ±0.10(10)

[a] The numbers in parentheses are the percentage absolute errors on σ_r.

where δ_{lj} are F-G scattering phase shifts, P_l are penetrabilities, $\phi_l = \tan^{-1}(f_l/g_l)$ are (neg) hard-sphere phase shifts (with f_l and g_l, the regular and irregular Coulomb functions) in the F-G channel, P_{C-D} is the penetration factor for particle D emission in the C-D channel, and C_{lj} are constants chosen to fit the data. Further, expressions capable of describing the shape of the continuous spectra for particles G that arise, as indicated in Eq. (1), from the secondary breakup of intermediate states of C, have been developed by Morinigo.[18] They depend on angular distributions in both the first-stage reaction and in the secondary breakup process. The energy spectrum $N_2(E)$ for particle G derived for the case of intermediate states C that have the shape of simple resonances is given in the Appendix.

The shape of the proton spectrum $N_1(E)$ calculated from Eq. (2) is shown as the solid curve in Fig. 10(a). In this example, the δ_{lj} are experimental α-α scattering phase shifts[19] for $(l=j) = 0, 2, 4$, and the corresponding quantities P_l and ϕ_l were calculated for a radius of 5 fm. The penetration factor P_{C-D} was calculated for s-wave proton emission in the p-^{8}Be channel with a radius of 4.35 fm. The constants C_{00} and C_{22} were chosen to fit the peak area and peak height, respectively, for the ground and 2.94-MeV states in ^{8}Be, while C_{44} had a value that reproduces the data in the region of the 11.4-MeV state (near $E_p \approx 8$ MeV). The incoherent addition of direct three-body breakup, as given by the three-body phase-space energy distribution,[20] fills in the valley near 12 or 13 MeV as indicated in Fig. 10(b). The inclusion of the contribution $N_2(E)$ from the secondary breakup of ^{5}Li into a proton and an α particle improves the agreement with the measurements as shown in Fig. 10(c). This calculation assumed that the angular distributions in both the first-stage reaction and the secondary decay were isotropic, and that the ^{5}Li ground state had the shape of a simple resonance with a width of 1.5 MeV.

Similar calculations reproduced quite acceptably the shape of the measured α-particle energy distributions (at energies $\gtrsim 3$ MeV), as indicated in the example of Fig. 11. The total spectrum (solid curve) represents an incoherent superposition of the partial contributions shown in Fig. 11. The contribution arising from p-α final-state interactions in the $p_{3/2}$ and $p_{1/2}$ states of ^{5}Li was calculated from Eq. (2) using experimental phase shifts.[21] Penetrabilities and hard-sphere phases in the p-α channel were obtained for a radius of 2.9 fm, while the penetration factors in the α-^{5}Li channel were determined for a radius of 4.12 fm. For contributions from the secondary breakup of ^{8}Be states, the angular distributions in the first-stage reaction [i.e., ^{6}Li(^{3}He, p)^{8}Be] were taken from the results of the present experiment (Sec. III); the angular distribution in the breakup of the ^{8}Be states was assumed isotropic. The secondary ^{5}Li breakup was accounted for by assuming isotropy in both stages of the reaction. All of the intermediate states (in ^{8}Be and ^{5}Li) were assumed to

TABLE II. Values of coefficients B_L in the expansion of the differential cross section for the ^{8}Be excited states and the continuum into a series of Legendre polynomials $[\sigma(\theta) = \sum_L B_L P_L (\cos\theta)]$, and the reaction cross sections σ_r, where $\sigma_r = 4\pi B_0$. The errors are relative uncertainties generated in the fitting program and do not include systematic errors.

$E_{^3He}$ (MeV)	B_0	B_1	B_2	B_3	B_4	σ_r[a] (mb)
			^{8}Be*(2.94 MeV) (mb/sr) (c.m.)			
0.660	0.076±0.008	0.005±0.012				0.96±0.10(18)
0.755	0.23 ±0.02	0.02 ±0.03	0.03±0.05			2.89±0.25(17)
0.849	0.45 ±0.01	0.06 ±0.02	0.04±0.02			5.65±0.13(14)
0.949	0.74 ±0.02	0.12 ±0.04	0.04±0.05			9.30±0.25(14)
1.063	1.16 ±0.03	0.32 ±0.06	0.05±0.08			14.6 ±0.4(14)
1.163	1.53 ±0.03	0.41 ±0.05	−0.26±0.08	−0.24±0.09		19.2 ±0.4(14)
1.271	1.74 ±0.11	0.39 ±0.16	−0.31±0.23	0.08±0.31		21.9 ±1.4(15)
1.370	1.74 ±0.05	0.40 ±0.08	−0.29±0.14	0.04±0.15		21.9 ±0.6(14)
1.470	1.86 ±0.07	0.20 ±0.11	0.21±0.16	−0.23±0.22		23.4 ±0.9(14)
1.568	2.29 ±0.01	−0.40 ±0.02	0.40±0.03	−0.76±0.05	0.20±0.05	28.8 ±0.1(14)
1.648	2.12 ±0.08	−0.17 ±0.09	−0.39±0.16	−0.77±0.21	0.44±0.26	26.6 ±1.0(14)
1.745	1.89 ±0.06	0.10 ±0.08	−0.38±0.11	−0.40±0.16	0.18±0.21	23.8 ±0.8(14)
1.847	2.11 ±0.14	−0.17 ±0.20	−0.24±0.31	−0.23±0.43	0.24±0.49	26.5 ±1.8(15.5)
			^{8}Be*(16.63 MeV)			
0.849	0.68 ±0.02	−0.06 ±0.04	−0.14±0.06			8.55±0.25(14)
0.949	0.63 ±0.03	−0.08 ±0.05	−0.26±0.07			7.92±0.38(14.5)
1.063	0.69 ±0.02	0.13 ±0.04	−0.10±0.06			8.67±0.25(14)
1.163	0.74 ±0.02	0.18 ±0.04	0.0 ±0.05			9.30±0.25(14)
1.271	0.94 ±0.03	0.13 ±0.05	−0.08±0.07			11.8 ±0.4(14)
1.370	1.07 ±0.04	0.06 ±0.07	−0.25±0.11			13.5 ±0.5(14)
1.470	1.19 ±0.05	0.21 ±0.08	−0.16±0.12			15.0 ±0.6(14)
1.568	1.20 ±0.04	0.22 ±0.07	−0.1 ±0.1			15.1 ±0.5(14)
1.648	1.26 ±0.05	0.51 ±0.09	0.07±0.13			15.8 ±0.6(14)
1.745	1.26 ±0.04	0.43 ±0.06	−0.12±0.09	−0.13±0.10		15.8 ±0.5(14)
1.847	1.49 ±0.06	0.2 ±0.1	0.09±0.16	−0.3 ±0.2		18.7 ±0.8(14.5)
			^{8}Be*(16.92 MeV)			
0.949	0.08 ±0.01	0.06 ±0.03				1.01±0.13(18.5)
1.063	0.24 ±0.03	0.23 ±0.07				3.02±0.38(18.5)
1.163	0.38 ±0.02	0.27 ±0.06	−0.21±0.07	−0.16±0.10		4.78±0.25(15)
1.271	0.51 ±0.04	0.31 ±0.08	−0.25±0.11	−0.24±0.13		6.41±0.50(16)
1.370	0.60 ±0.04	0.46 ±0.09	0.04±0.12	0.08±0.12		7.54±0.50(15)
1.470	0.67 ±0.05	0.49 ±0.10	−0.04±0.13	−0.14±0.17		8.42±0.63(15.5)
1.568	0.97 ±0.04	0.47 ±0.08	0.05±0.11	0.23±0.12		12.2 ±0.5(14.5)
1.648	0.72 ±0.04	0.22 ±0.06	−0.23±0.10	−0.14±0.11		9.05±0.50(14.5)
1.745	0.70 ±0.05	0.34 ±0.14	−0.08±0.14	−0.23±0.26		8.80±0.63(15.5)
1.847	0.85 ±0.03	0.42 ±0.06	0.07±0.08	0.1 ±0.1		10.7 ±0.4(14.5)
			Continuum (mb/sr) (lab)			
0.660	0.47 ±0.03	−0.03 ±0.06	0.09±0.07			5.98±0.38(15.5)
0.755	1.44 ±0.14	0.43 ±0.25	0.03±0.32			18.1 ±1.8(16)
0.849	2.72 ±0.05	0.71 ±0.11	0.79±0.13			34.2 ±0.6(14)
0.949	3.68 ±0.09	0.96 ±0.18	1.04±0.23			46.2 ±1.1(14)
1.063	5.08 ±0.12	1.53 ±0.23	1.39±0.29			63.8 ±1.5(14)
1.163	5.57 ±0.21	1.64 ±0.39	1.30±0.45			70.0 ±2.6(14)
1.271	6.40 ±0.24	2.13 ±0.49	1.31±0.60			80.4 ±3.0(14)
1.370	6.54 ±0.24	2.64 ±0.47	1.34±0.58			82.2 ±3.0(14)
1.470	6.4 ±0.2	1.37 ±0.37	1.67±0.48			80.4 ±2.5(14)
1.568	7.24 ±0.15	2.24 ±0.30	1.04±0.35			90.9 ±1.9(14)
1.648	6.59 ±0.29	2.43 ±0.48	0.98±0.58			82.8 ±3.6(14.5)
1.745	6.38 ±0.34	2.87 ±0.62	1.37±0.75			80.2 ±4.3(15)
1.847	7.00 ±0.44	1.63 ±0.81	0.5 ±1.1			88.0 ±5.5(15.5)

[a] The numbers in parentheses are the percentage absolute errors on σ_r.

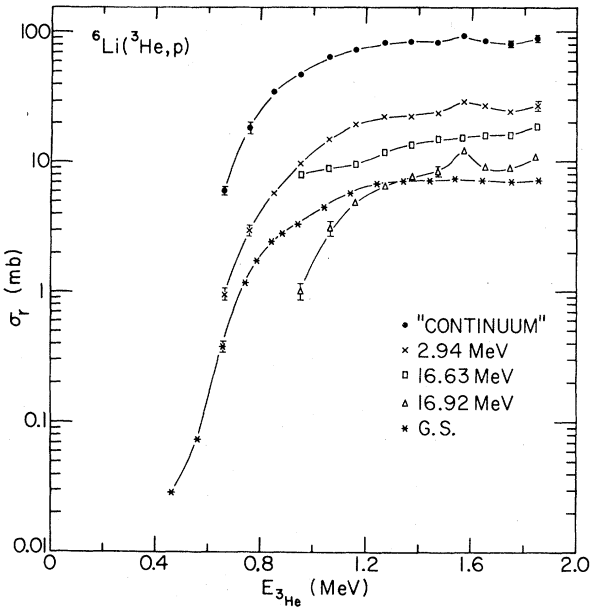

FIG. 7. Integrated cross sections ($\sigma_r = 4\pi B_0$) for the protons from the ^{3}He+^{6}Li reactions. The solid lines are to guide the eye. The error bars represent the relative accuracies of the measurements.

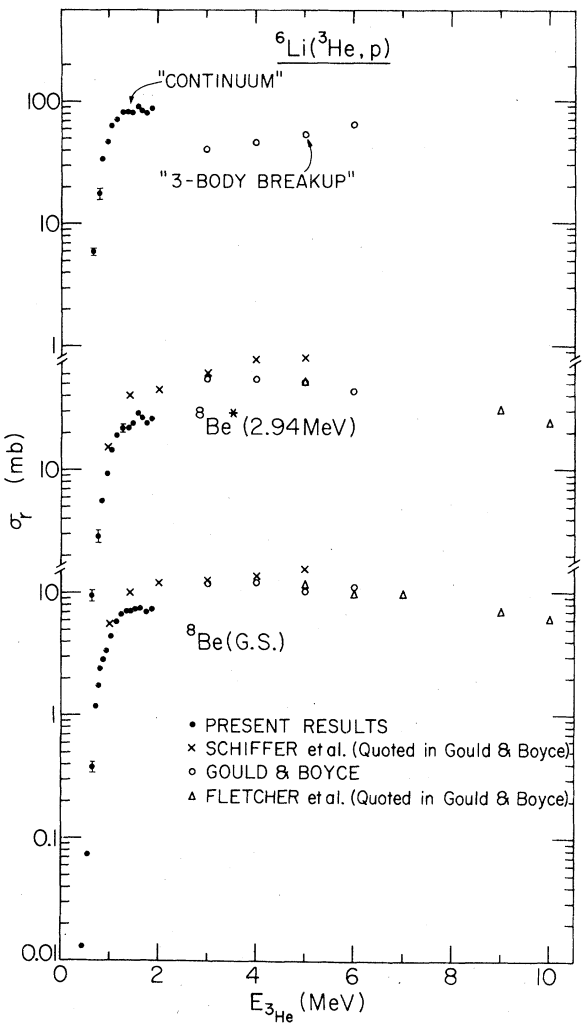

FIG. 8. Integrated cross sections ($\sigma_r = 4\pi B_0$) for the protons from the ^{3}He+^{6}Li reactions compared to previous measurements, Refs. 8–10. The results of Ref. 10 for the 2.94-MeV state have been normalized to those of Ref. 9.

have the shape of simple resonances with widths taken from the compilation of Ajzenberg-Selove.[22]

The good agreement in these examples between measured and calculated spectral shapes suggest that the production of protons and α particles in ^{3}He + ^{6}Li reactions arises predominantly from sequential reactions through the known[22] states of ^{8}Be and ^{5}Li with only a small contribution from direct three-body breakup. A contribution from any other, as yet unknown, energy level in ^{8}Be below 17-MeV excitation is unlikely unless such a state were extremely broad.

B. Thermonuclear reaction-rate parameters

The primary nuclear reactions of an advanced p-^{6}Li fusion fuel cycle[5] include the ^{6}Li(^{3}He, p) and ^{6}Li(^{3}He, d) reactions as well as ^{6}Li(p, ^{3}He) process. A complete determination of the feasibility of such a fuel cycle requires (among other things) a knowledge of the reaction rate parameters $\langle\sigma v\rangle$ for each process, where σ is the reaction cross section, v the relative velocity between the interacting nuclei, and the average is taken over a Maxwell-Boltzmann distribution of velocities.

We have calculated reaction-rate parameters for the various branches of the ^{6}Li(^{3}He, p) reaction by the method discussed by Elwyn *et al.*[23] In this analysis, the reaction cross sections listed in Tables I and II were used from ~0.5 to 1.85 MeV, along with those given in Refs. 8–10 from 2.0 to 10 MeV for the ground and 2.94-MeV ^{8}Be states. The cross sections at energies higher than those measured were assumed equal to the values at the highest measured point. Since no data exist at energies less than ~0.5 MeV, the calculated values of $\langle\sigma v\rangle$ will be somewhat uncertain at low temperatures (i.e., at low values of kT). In Fig. 12, $\langle\sigma v\rangle$ is calculated on the assumption (a) that reaction cross sections are zero at all energies below the region of the data and (b) with low-energy cross sections obtained by extrapolation to zero from the value at the lowest energy data point by use of the formula Eq. (2.21) given by Monahan *et al.*[24]

These limits serve as estimates of the uncertainties in the calculated rates. Note that for

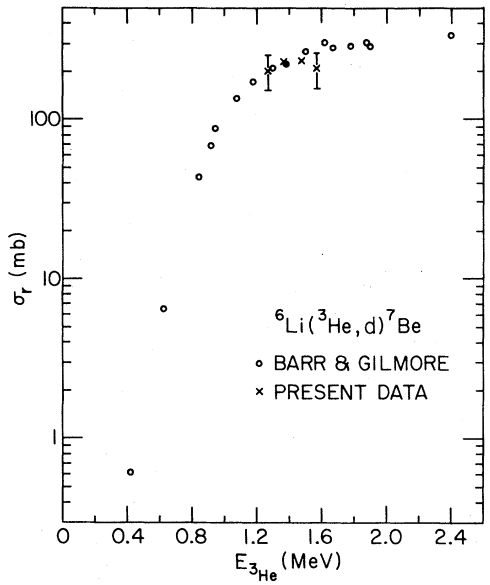

FIG. 9. Reaction cross sections for the ^{6}Li(^{3}He,d)^{7}Be reaction. The results of Barr and Gilmore (Ref. 16) are based on an activation technique. The absolute errors on the results of the present work are estimated to be ±25%.

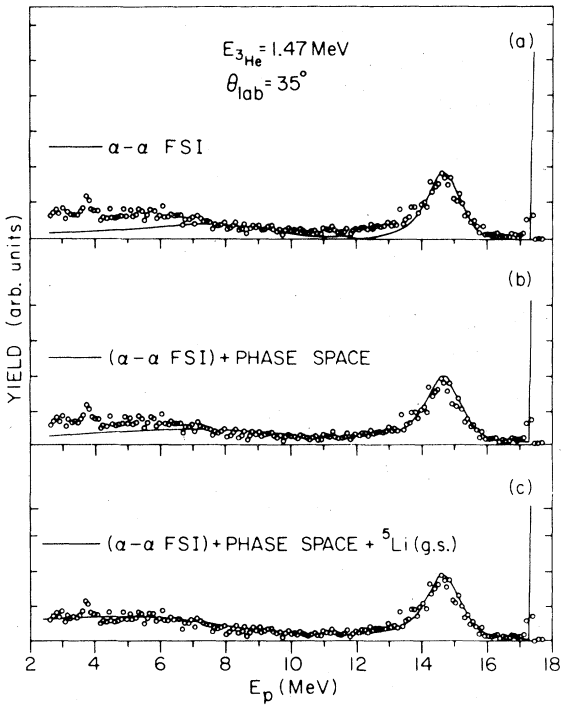

FIG. 10. Energy spectrum of the protons in ^{3}He+^{6}Li reactions at $E_{^3He}$ = 1.47 MeV and θ_{lab} = 35°. Calculations of the spectral shape based on Eq. (2) in the text (as described in the text) is shown as the solid line in (a). The effect of the incoherent addition of direct three-body breakup is indicated in (b). The addition of the contribution from the secondary breakup of ^{5}Li (see text and Appendix) leads to the final calculation shown in (c).

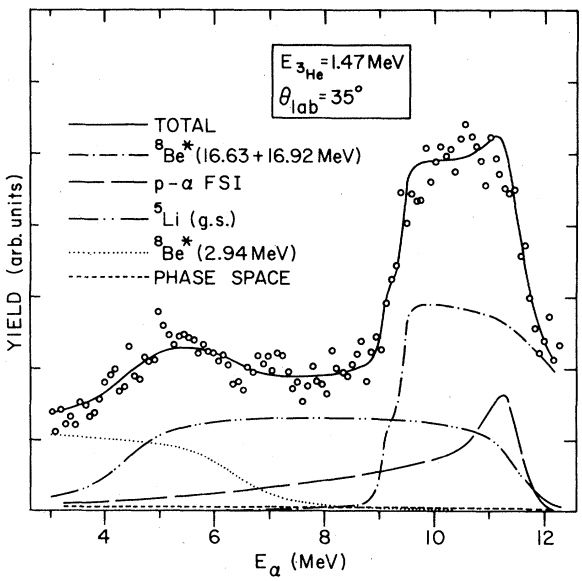

FIG. 11. Energy spectrum of the α particles in ^{3}He + ^{6}Li reactions at $E_{^3He}$ = 1.47 MeV and θ_{lab} = 35°. The solid curve represents the incoherent superposition of the partial contributions shown. The contributions marked p-α FSI represent a calculation based on Eq. (2) in the text, while those marked ^{8}Be*(2.94), ^{8}Be*(16.63 + 16.92), and ^{5}Li(g.s.) are calculations based on Eq. (A15) as discussed in the text and Appendix. The phase space contribution is based on an expression given, for example, in Ref. 20.

$kT \gtrsim 200$ keV, the two calculations are equal. Reaction rate parameters calculated with the extrapolated cross sections of method (b) above are tabulated for each of the ^{6}Li(^{3}He,p) reaction channels in Table III, and plotted as a function of temperature in Fig. 13.

McNally *et al.*[25] have tabulated reaction-rate parameters for a large number of light-isotope reactions based on previously published data. The values for the ^{6}Li(^{3}He,p) reaction are, as seen in Fig. 14, smaller, by about a factor of 4, than the sum of the individual contributions based on the present work. The extent to which the new $\langle\sigma v\rangle$ values presented here enhance the potential of the p-^{6}Li fusion fuel cycle remains to be determined.

ACKNOWLEDGMENTS

We would like to thank R. Amrein and the operating staff of the Dynamitron accelerator for their cooperation in performing the measurements reported here. The encouragement of Prof. R. W. Conn and Dr. J. Rand McNally is appreciated. This work was performed under the auspices of the U. S. Department of Energy.

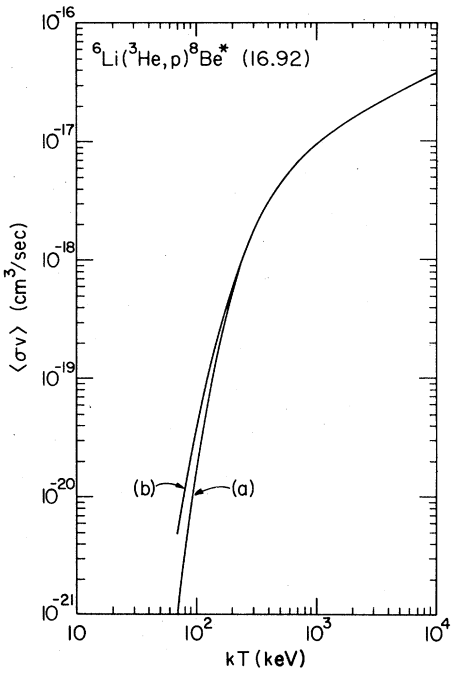

FIG. 12. Reaction rate parameters $\langle\sigma v\rangle$ as a function of kT for the ^{6}Li(^{3}He,p)^{8}Be*(16.92-MeV) reaction calculated on the assumption (a) that the reaction cross sections are zero at all energies below the lowest energy data point, and (b) with low-energy cross sections obtained by use of the extrapolation formula given in Rev. 24, as discussed in the text.

APPENDIX

As described in Sec. IV we have made use of the formalism of Morinigo[18] to describe the spectrum of particles G coming from the secondary breakup of a sequential two-stage reaction

$$A+B\rightarrow C+D$$
$$\qquad\quad \hookrightarrow F+G\,. \tag{A1}$$

Because the general case we consider is not treated explicitly in Ref. 18 and because some of our intermediate results seem to differ from the equations given in this reference, a brief description of the formalism used in the present analysis is given below.

Let m_x denote the mass of particle X and define the following vectors: $\vec{g}$, the velocity of G in the laboratory system; $\vec{u}$, the velocity of the center of mass of the entire system relative to the laboratory; $\vec{v}$, the velocity of C in the center-of-mass system; and $\vec{w}$, the velocity of G relative to C. The geometric relations of these vectors is shown in Fig. 15. It is also convenient to define the following quantities:

$$a=-u^2-g^2+2ugz\,, \tag{A2}$$

$$b=2(gz-u)(v+wy_0)\,, \tag{A3}$$

$$c=w^2(1-y_0^2)-(gz-u)^2\,, \tag{A4}$$

TABLE III. Reaction rate parameters $\langle\sigma v\rangle$ for the ^{6}Li(^{3}He,p) reaction.

kT (MeV)	^{8}Be(g.s.)	^{8}Be*(2.94)	^{8}Be*(16.63)	^{8}Be*(16.92)	Continuum
		(cm^3 sec^{-1})			
0.01	5.78E-28[a]	3.08E-27	1.33E-26	7.47E-28	1.92E-26
0.02	6.10E-25	3.23E-24	1.18E-23	7.81E-25	2.01E-23
0.03	1.73E-23	8.83E-23	2.80E-22	2.13E-23	5.50E-22
0.04	1.59E-22	7.03E-22	1.92E-21	1.65E-22	4.37E-21
0.05	8.48E-22	3.12E-21	7.22E-21	6.93E-22	1.92E-20
0.06	3.06E-21	9.84E-21	1.91E-20	2.08E-21	5.90E-20
0.07	8.25E-21	2.46E-20	4.06E-20	5.03E-21	1.43E-19
0.08	1.80E-20	5.19E-20	7.41E-20	1.05E-20	2.89E-19
0.09	3.39E-20	9.61E-20	1.21E-19	1.97E-20	5.16E-19
0.1	5.70E-20	1.61E-19	1.83E-19	3.37E-20	8.33E-19
0.2	7.29E-19	2.28E-18	1.56E-18	5.79E-19	8.79E-18
0.3	1.98E-18	6.78E-18	3.74E-18	1.72E-18	2.09E-17
0.4	3.45E-18	1.26E-17	6.08E-18	3.05E-18	3.30E-17
0.5	4.88E-18	1.87E-17	8.30E-18	4.35E-18	4.39E-17
0.6	6.19E-18	2.45E-17	1.03E-17	5.55E-18	5.37E-17
0.7	7.36E-18	2.99E-17	1.22E-17	6.65E-18	6.24E-17
0.8	8.39E-18	3.47E-17	1.39E-17	7.65E-18	7.03E-17
0.9	9.28E-18	3.90E-17	1.54E-17	8.56E-18	7.74E-17
1.0	1.01E-17	4.27E-17	1.69E-17	9.40E-18	8.40E-17
2.5	1.52E-17	6.57E-17	3.11E-17	1.77E-17	1.50E-16
5.0	1.81E-17	7.56E-17	4.53E-17	2.59E-17	2.16E-16
7.5	2.04E-17	8.39E-17	5.58E-17	3.19E-17	2.66E-16
10.0	2.27E-17	9.22E-17	6.46E-17	3.69E-17	3.08E-16

[a] Read as 5.78×10^{-28}.

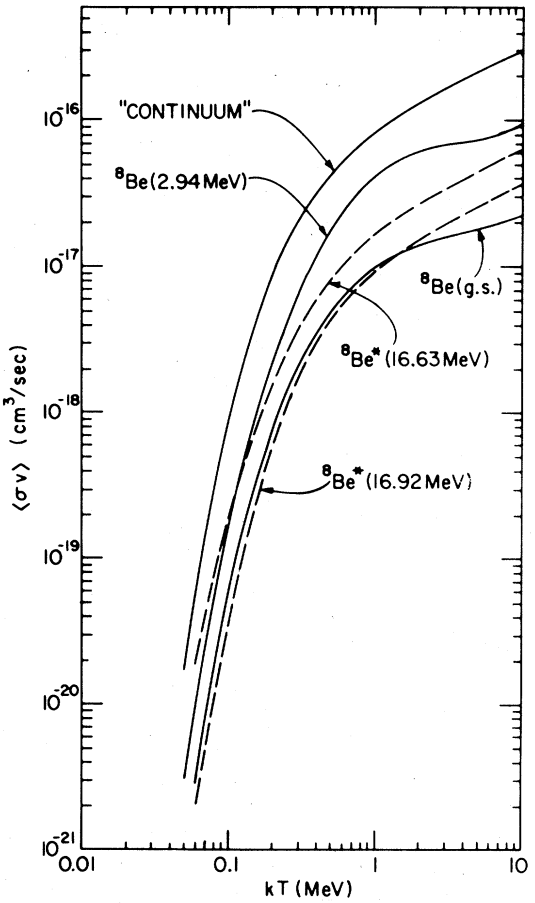

FIG. 13. Reaction rate parameters $\langle\sigma v\rangle$ as a function of kT for the various outgoing proton channels in ^{3}He + ^{6}Li reactions calculated as discussed in the text.

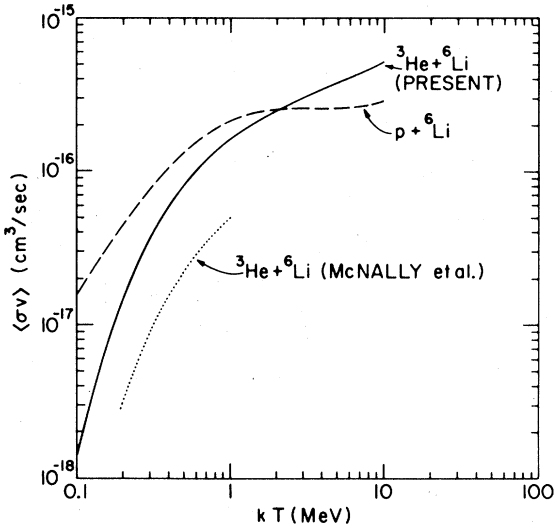

FIG. 14. Comparison of $\langle\sigma v\rangle$ for the sum of the various outgoing proton channels compared to previous results (Ref. 25). Also shown are results for the ^{6}Li(p,^{3}He)^{4}He reaction (Ref. 3).

$$y_0 = -(a+v^2+w^2)/(2vw)\,, \tag{A5}$$

$$w = [\mu(v_0^2 - v^2)]^{1/2}\,, \tag{A6}$$

$$\mu = [m_C m_F(m_D+m_C)]/[m_D m_G(m_G+m_F)]\,, \tag{A7}$$

$$v_0^2 = \frac{2m_D}{m_C(m_C+m_D)}\left(Q+\frac{m_B E}{m_A+m_B}\right)\,, \tag{A8}$$

where $\cos^{-1}z$ is the laboratory angle of observation of G, E is the laboratory energy of the incident particle A, and Q is the overall energy released in the reaction (A1). The distribution in energy and angle of particles G in the laboratory system is given by Eq. (28) of Ref. 18:

$$\frac{d^2\sigma}{dE_g\,dz} = \frac{8\pi m_F \sigma g}{m_G^2(m_G+m_F)} \int_{v'}^{v''} dv\, vW(\vec{w}) \times \int_{x'}^{x''} dx\, \frac{W'(x)}{(ax^2+bx+c)^{1/2}}\,, \tag{A9}$$

where σ is the total cross section for the first-step reaction in (A1), $W(\vec{w})$ is the probability distribution of the velocity vector $\vec{w}$, $W'(x)$ is the angular distribution of particles C in the center-of-mass system, and x is the cosine of the center-of-mass angle of emission of particles C. The limits of integration $x' < x''$ are roots of $ax^2+bx+c=0$ and v', v'' are the roots

$$\{\pm t \pm [\mu(1+\mu)v_0^2 - \mu t^2]^{1/2}\}/(1+\mu)\,, \tag{A10}$$

which fall in the interval $0 < v' < v'' < v_0$. Here, $t = (-a)^{1/2}$.

We now assume that the reaction (A1) proceeds through a resonance in particle C, i.e., we take $W(\vec{w})$ to have the form

$$W(w) = [(w^2 - w_R^2)^2 + \rho^2]^{-1}\,, \tag{A11}$$

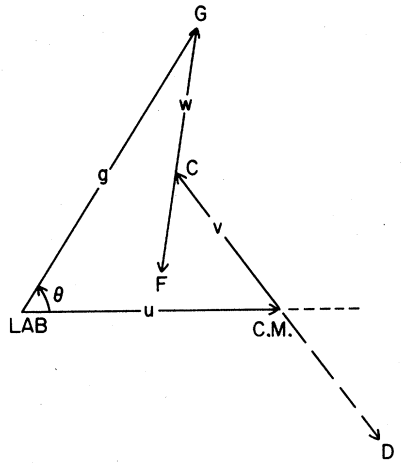

FIG. 15. Geometric relations of the velocity vectors $\vec{u}$, $\vec{v}$, $\vec{w}$, and $\vec{g}$ for the reaction $A+B \rightarrow C+D \rightarrow F+G+D$, as discussed in the Appendix.

where w is defined in terms of v by Eq. (A6). Here we have assumed that the angular distribution of particles G are isotropic in the rest frame of C. Next expand the angular distribution of particles C in powers of x, i.e.,

$$W'(x) = 1 + \alpha x + \beta x^2 . \tag{A12}$$

The integration over x in Eq. (A9) can then be carried out to give

$$\frac{d^2\sigma}{dE_g\,dz} = \frac{8\pi^2 m_F \sigma g}{m_G^2 (m_G + m_F)} \frac{1}{(-a)^{1/2}} \int_{v'}^{v''} \frac{dv\, v}{\left[\mu(v^2 - v_0^2) + w_R^2\right]^2 + \rho^2} \left(1 - \alpha \frac{b}{2a} + \beta \frac{3b^2 - 4ac}{8a^2}\right) . \tag{A13}$$

The integration over v in Eq. (A13) is approximated as follows. Consider the integral

$$I(i,j) = \int_i^j \frac{dv\, v}{\left[\mu(v^2 - v_0^2) + w_R^2\right]^2 + \rho^2} = \frac{1}{2\mu\rho} \left[\tan^{-1} \frac{\mu(j^2 - v_0^2) + w_R^2}{\rho} - \tan^{-1} \frac{\mu(i^2 - v_0^2) + w_R^2}{\rho}\right] . \tag{A14}$$

In terms of this integral Eq. (A13) can be evaluated approximately as

$$N_2(E) \equiv \frac{d^2\sigma}{dE_g\,dz} = \frac{8\pi^2 m_F \sigma g}{m_G^2 (m_G + m_F)} \frac{1}{(-a)^{1/2}} \left[I(v', v'') - \frac{\alpha}{2a} \sum_{j=1}^{n} b_j I(v_{j-1}, v_j) + \frac{\beta}{8a^2} \sum_{j=1}^{n} (3b^2 - 4ac)_j I(v_{j-1}, v_j)\right] , \tag{A15}$$

where $v_{j-1} < v_j$ and $v_0 = v'$, $v_n = v''$. In Eq. (A15), b_j is evaluated using Eq. (A3) and $(3b^2 - 4ac)_j$ using Eqs. (A2)–(A4) for a value of v satisfying the inequality $v_{j-1} < v < v_j$.

[1] A. J. Elwyn, R. E. Holland, C. N. Davids, L. Meyer-Schützmeister, J. E. Monahan, F. P. Mooring, and W. Ray, Jr., Phys. Rev. C 16, 1744 (1977).

[2] R. E. Holland, A. J. Elwyn, C. N. Davids, F. J. Lynch, L. Meyer-Schützmeister, J. E. Monahan, F. P. Mooring, and W. Ray, Jr., Phys. C 19, 592 (1979).

[3] A. J. Elwyn, R. E. Holland, C. N. Davids, L. Meyer-Schützmeister, F. P. Mooring, and W. Ray, Jr., Phys. Rev. C 20, 1984 (1979).

[4] See, e.g., a number of articles in *Proceedings of the Review Meeting on Advanced-Fuel Fusion*, EPRI ER-536-SR (Electric Power Research Institute, Palo Alto, 1977).

[5] R. W. Conn and G. Shuy, University of Wisconsin, Report No. UWFDM-262, 1979 (unpublished); G. W. Shuy and R. W. Conn, in *Proceedings of the International Conference on Nuclear Cross Sections and Technology*, Knoxville, Tennessee, 1979 (to be published).

[6] Rand McNally, in *Abstracts from the 1979 IEEE International Conference on Plasma Science, Montreal, 1979*, Report No. 79CH1410-0 NPS (IEEE Service Center, Piscataway, N. J., 1979), p. 52.

[7] See, for example, D. A. Bromley and E. Almquist, Chalk River Report No. CRP-881 AECL 950, 1959 (unpublished).

[8] J. P. Schiffer, T. W. Bonner, R. H. Davis, and F. W. Prosser, Jr., Phys. Rev. 104, 1064 (1956).

[9] C. R. Gould and J. R. Boyce, Nucl. Sci. Eng. 60, 477 (1976).

[10] N. R. Fletcher, J. D. Marshall, and R. H. Davis, Nucl. Phys. 70, 471 (1965).

[11] J. R. Erskine and C. P. Browne, Phys. Rev. 123, 958 (1961).

[12] J. B. Marion, Rev. Mod. Phys. 38, 660 (1966).

[13] H. H. Andersen and J. F. Ziegler, *The Stopping and Ranges of Ions in Matter* (Pergamon, New York, 1977), Vol. 3; J. F. Ziegler, *The Stopping and Ranges of Ions in Matter* (Pergamon, New York, 1977), Vol. 4.

[14] A narrow state in ^{8}Be at an excitation of 17.64 MeV can be excited at ^{3}He bombarding energies greater than ~1.4 MeV, and would lead to the existence of a low-energy peak in the proton spectrum. Such a peak was not observed in the present experiment.

[15] The average ^{3}He bombarding energy $E_{^3\mathrm{He}}$ was calculated by use of the approximate expression $E_{^3\mathrm{He}} = E^{\mathrm{INC}}_{^3\mathrm{He}} - \frac{1}{2}\Delta$, where Δ is the target thickness (in energy units) obtained from tabulated atomic stopping powers (Ref. 13) at the energy $E^{\mathrm{INC}}_{^3\mathrm{He}}$. The average energies were identical to within ~1 keV at all incident energies used in the present experiment with those based on the more accurate calculations discussed in Ref. 1.

[16] D. W. Barr and J. S. Gilmore, private communication (1965).

[17] F. C. Barker and P. B. Treacy, Nucl. Phys. 38, 33 (1962).

[18] F. B. Morinigo, Nucl. Phys. A127, 116 (1969).

[19] See, e.g., S. A. Afzal, A. A. Z. Ahmad, and S. Ali, Rev. Mod. Phys. 41, 247 (1969); A. D. Bacher, F. G. Resmini, H. E. Conzett, R. de Swiniarski, H. Meiner, and J. Ernst, Phys. Rev. Lett. 29, 1331 (1972).

[20] G. G. Ohlsen, Nucl. Instrum. Methods 37, 240 (1965).

[21] D. C. Dodder, G. M. Hale, N. Jarmie, and K. Witte, Los Alamos Sci. Lab. Report No. LA-6389MS, 1976 (unpublished); D. C. Dodder, G. M. Hale, N. Jarmie, J. H. Jett, P. W. Keaton, Jr., R. A. Nisley, and K. Witte, Phys. Rev. C 15, 518 (1977).

[22] F. Ajzenberg-Selove, Nucl. Phys. A320, 1 (1979).

[23] A. J. Elwyn, J. E. Monahan, and F. J. D. Serduke, Nucl. Sci. Eng. 63, 343 (1977).

[24] J. E. Monahan, A. J. Elwyn, and F. J. D. Serduke, Nucl. Phys. A269, 61 (1976). The procedure is discussed in some detail in this reference. The extra-

polation formula $\sigma = (S/E) \exp(-2\pi Z_1 Z_2 e^2/\hbar v)$, customarily employed in such calculations, is an approximation to the more rigorous expression derived in this reference. See also the discussion in Sec. IV A of Ref. 3.

[25]J. Rand McNally, Jr., K. E. Rothe, and R. D. Sharp, Oak Ridge National Lab Report No. ORNL/TM-6914. 1979 (unpublished).